Proceedings of the
4th JSME-KSME Thermal Engineering Conference
October 1-6, 2000, Kobe, Japan

B312

SIMULATIONS OF THREE-DIMENSIONAL COMBUSTION CHARACTERISTICS IN A REVERSE FLOW ANNULAR GAS TURBINE COMBUSTOR

Nahm Roh Joo*, Ho Young Kim* , Jin Taek Chung* and Seong Ki Min**

*Department of Mechanical Engineering, Korea University
1, 5-ka, Anam-dong, Sungbuk-ku, Seoul, 136-701, Korea

**Agency for Defense Development
3-ASM-4, Yuseong P.O.Box 35-3, Taejon, 305-600, Korea

ABSTRACT This paper presents the three dimensional modeling of the combustion flow field in a reverse flow annular gas turbine combustor. Calculations are performed at 20° sector of the combustion chamber including the dilution holes and liner film cooling slots. The standard $k-\varepsilon$ model is used for the turbulent flow. Combustion characteristics are predicted using an assumed β-PDF of fast chemistry. Two configurations of primary holes are examined in order to investigate its influence on the combustion flow field. Results provide that the configuration in which the primary jets are located in the midplane shows good jet mixing. Simulations are also carried out for the two operating conditions with various fuel mass flowrates. It is found that as the mass flowrate of fuel increases, the average exit temperature increases, whereas the temperature in primary zone reaches a maximum value under near stoichiometric condition. The predicted exit gas temperatures are compared with the corresponding experimental data and show good agreement.

Keywords: reverse flow annular combustor, gas turbine, two phase flow, fast chemistry, pattern factor

1. INTRODUCTION

For many small gas turbine engines, close coupling of the compressor and turbine is necessary to alleviate shaft whirling problems. This requirement has led to the use of the annular reverse flow combustor. As in a conventional annular combustor, flame is stabilized by the recirculation flow in the primary zone. This is generated by the combination of an axial swirling air jet associated with fuel injection and a radial air jet in the primary zone. Hot combustion products leaving the intermediate zone are diluted by the cooling air in the dilution zone. For reverse flow combustors, the dilution zone is connected to the bend that turns the flow 180° into the turbine. Figure 1 shows the schematic of the reverse flow annular gas turbine combustor.

Fuller et al. [1] demonstrated the CFD modeling techniques for gas turbine combustors by using the multi-domain calculations. The prediction of the flow field in a gas turbine combustor can require the consideration of two phases, especially under low power conditions. However, under high power conditions the fuel may be assumed to be in a fully vaporized state. Tolpadi [2] showed a better agreement with the experimental data in the case of two-phase analysis compared with the case of fully vaporized state. Tolpadi et al. [3] considered finite rate chemistry effects via a multiple scalar scheme for the fuel. Crocker et al. [4] performed the CFD calculation for a full model combustor from the compressor exit to the turbine inlet implementing a one-step finite rate reaction with equilibrium reaction products. Fractions of mass flows and inlet conditions for openings into the combustor liner as well as liner wall temperature were described.

In addition to the reaction chemistry, an accurate prediction of the flow through the nozzle/swirler is essential. Fuller and Smith [5] estimated velocity profiles at the swirler exit by using 2-D analysis and applied to 3-D combustor simulations. Tolpadi et al. [6] obtained the gas phase flow field and the spray characteristics for an engine swirl cup. Rizk [7] performed the spray modelings for air-blast and air-assist atomizers. Datta and Som [8] studied the effects of mean droplet diameter and spray cone angle on the characteristics of combustion within a gas turbine combustor. They found that an increase of each parameter decreased the pattern factor. For a reverse flow combustor, Crocker et al. [9] performed experimental studies to enhance the mixing of dilution zone. It was found that the angled dilution jets injecting with a high circumferential velocity component reduced the pattern factor.

Although many studies have been carried out for a conventional annular gas turbine combustor, numerical predictions on the reverse flow combustor considering liner film cooling slots have not been completed. The prime objectives of the present study are to describe the jet mixing effects on the temperature distributions using a two-phase analysis in the reverse flow combustor and to give comparatively accurate predictions of the temperature at combustor exit. Two configurations of primary hole are

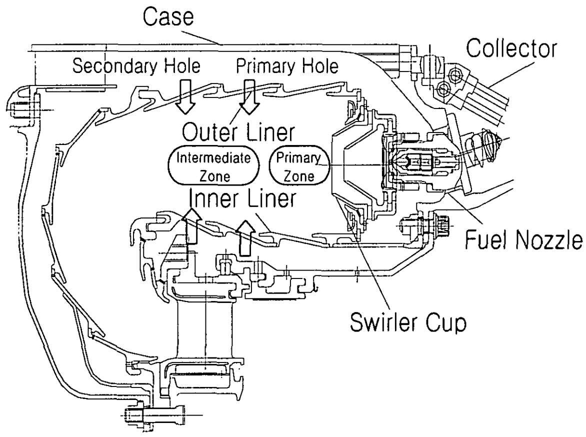

Fig.1 Schematic of reverse flow annular combustor

examined in order to predict the influences on the combustion field. In addition, the effects of fuel mass flowrate on the flow field of primary zone are also studied.

2. THEORETICAL MODELS

2.1 Gas Phase

The general form of the three-dimensional conservation equations may be written for a variable ϕ in Cartesian coordinates as follows:

$$\frac{\partial}{\partial x}(\rho u\phi)+\frac{\partial}{\partial y}(\rho v\phi)+\frac{\partial}{\partial z}(\rho w\phi)=\frac{\partial}{\partial x}(\Gamma\frac{\partial\phi}{\partial x})+\frac{\partial}{\partial y}(\Gamma\frac{\partial\phi}{\partial y})+\frac{\partial}{\partial z}(\Gamma\frac{\partial\phi}{\partial z})+S \tag{1}$$

where ρ is the fluid density, Γ is the effective diffusion coefficient, u, v and w are the three Cartesian velocity components, and S is the source term including the interactions with particles. Turbulent flow is modeled using the standard $k-\varepsilon$ model along with the wall function treatment for near wall regions. Conserved scalar variable for the fuel mixture fraction with an assumed β-PDF (Probability Density Function) of a fast chemistry is used for the combustion modeling. $C_{12}H_{23}$ (kerosene) is used as a fuel in this study.

2.2 Liquid Phase

When the liquid fuel is injected into the combustor as a spray, the equation of motion of a spherical droplet may be written in the following form:

$$d\vec{u}_\ell/dt=(\vec{u}-\vec{u}_\ell)/\tau_d \tag{2}$$

where $\vec{u}_\ell$ is velocity of droplet and $\vec{u}$ is sum of the mean velocity of gas phase and the fluctuating velocity that is chosen randomly from an isotropic Gaussian distribution. Dynamic relaxation time τ_d is defined as

$$\tau_d=4\rho_\ell d^2/(3\mu C_D\,\mathrm{Re}) \tag{3}$$

In this study, drag coefficient C_D is chosen from Morsi and Alexander [10]:

$$C_D=a_1+a_2/\mathrm{Re}+a_3/\mathrm{Re}^2 \tag{4}$$

During the heat-up period, the droplet temperature can be obtained from the energy equation including the convective and radiative heat transfers between the droplets and the gas phase.

$$m_\ell C_{p\ell}\frac{dT_\ell}{dt}=hA_\ell(T_\infty-T_\ell)+h_{fg}\frac{dm_\ell}{dt}+A_\ell\varepsilon_\ell\sigma(\theta_R^4-T_\ell^{\,4}) \tag{5}$$

When the temperature of the droplet reaches the boiling temperature, it remains constant and the evaporation rate can be calculated from eq. (5).

2.3 Pattern factor

The dilution jets should be effectively mixed with the combustion gases, thereby establishing an appropriate radial temperature profile and an acceptable maximum temperature. Reducing the maximum temperature for the fixed average temperature at combustor exit can improve the safety of turbine inlet guide vanes. The expression used to describe the maximum temperature, known as the pattern factor (PF), is defined as

$$\mathrm{PF}=(T_{\max}-T_{ex})/(T_{ex}-T_{in}) \tag{6}$$

3. NUMERICAL MODELS

The combustion flow field of a modern reverse flow annular gas turbine combustor is analyzed in this study. There are 36 primary holes on the outer and inner liners, respectively. 72 secondary holes zigzaging on the outer liner are assumed to be in line, and 36 secondary holes on the inner liner have larger diameters. In addition, there are ten and seven liner film cooling slots on the outer and inner liners, respectively. The combustor is annular with 18 swirl cups equally spaced along the circumferential direction. Within a single-cup sector of 20° span, there are pertinent dilution holes (primary and secondary) and liner film cooling slots on both the outer and inner liners.

Two configurations of primary hole are analyzed as shown in Fig.2 in order to compare the combustion characteristics. Note that the holes are located with the same span. Experimental data [11] presented in this paper are obtained for the configuration 1. Based on its results, numerical data for the configuration 2 are used for the comparison of jet mixing effects on the temperature distributions.

The liner film cooling slots are modeled using a rearward-facing step technique. In this multi-domain grid, each domain is larger than the preceding domain creating the stepwise slots with normal inlet boundary conditions. These calculations eliminate the waste cells commonly associated with single-domain calculations. Furthermore,

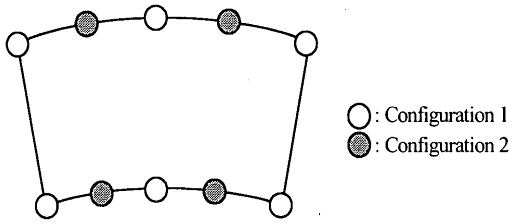

Fig.2 Primary hole configurations examined

Table 1. Operating conditions

Case	Pressure	Temperature	Air mass flow
Case 1	5.8 bar	584K	2.33 kg/s
Case 2	13.7 bar	687K	5.43 kg/s

periodic boundary conditions are imposed on the two side planes.

The fractions of the air mass flowrates through the swirler, primary holes, secondary holes, and liner cooling slots are 13, 16, 33, and 38 percent, respectively. The droplet size distribution is given by the Rosin-Rammler function. Five size ranges from 10 to 60 microns are selected with a SMD of 30 microns. Initial droplet velocities are assumed to be the same as the corresponding local air velocities, which are obtained from experiment [12]. Calculations for various fuel mass flowrates are performed at two operating conditions as shown in Table 1.

4. RESULTS

Figure 3(a) presents the velocity vectors on the cross-sectional plane downstream of the swirler. The velocity vectors and streamlines on the side view midplane along the centerline of swirler are shown in Fig.3 (b) and (c) for two configurations. In both configurations, two weak recirculation zones are generated in the combustor primary zone. A central recirculation zone (CRZ) is created along the swirler centerline, and dome recirculation zone (DRZ) is caused by the sudden expansion of the swirler airflow discharging into the combustor. In the case of configuration 1, penetration of air jets from the primary and secondary holes can be clearly observed. The jets from the primary holes are forced into the primary zone while the opposed jets from the secondary holes impinge upon each other. In the case of configuration 2, however, swirling motion from the swirler reaches the jets from the secondary holes directly. The flow acceleration toward the exit of the combustor is shown in both configurations.

The effect of turbulence on the droplet motion is considered using a stochastic approach. Figure 4 shows the trajectories of fuel droplets. To avoid cluttering up this figure, only a few deterministic trajectories are depicted. Since droplets are heated up and evaporated along the trajectories, they show the distance traversed by the liquid fuel droplets before complete evaporation. All droplets are observed to evaporate completely within the primary zone.

Figure 5 shows the contours of the fuel mass fraction for various equivalence ratios on the top-view midplane. The sum of the air flowrates from the swirler and primary hole is used for the definition of the equivalence ratio in the primary zone. These figures show the existence of fuel rich regions downstream of the swirler. Furthermore, as the droplets travel farther downstream, the fuel concentration is spread over a wider region. The rapid reduction of fuel concentration can be observed in the vicinity of the radial air jets from primary holes. Unburned fuels passing by the opposed jets remain within the intermediate zone. As the fuel mass flow increases, the fuel concentration in the primary zone increases, and the unburned fuel reaches farther downstream. In the case of configuration 2, the fuel rich core region reaches the opposed air jets from the secondary hole.

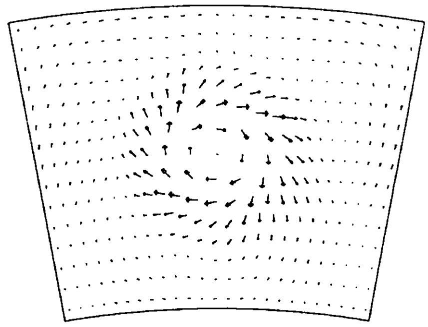

(a) cross-sectional plane

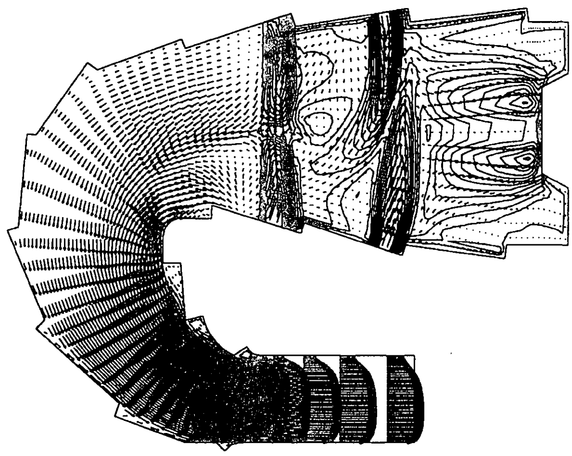

(b) side-view midplane for configuration 1

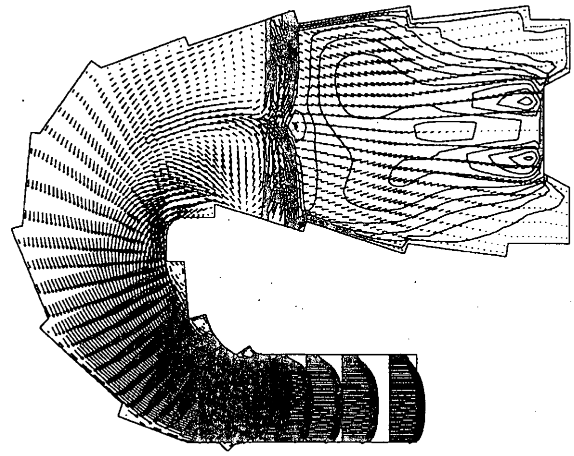

(c) side-view midplane for configuration 2

Fig. 3 Flow fields in reverse flow annular combustor

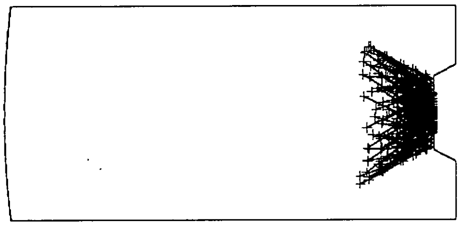

Fig. 4 Droplet trajectories projected on top-veiw midplane

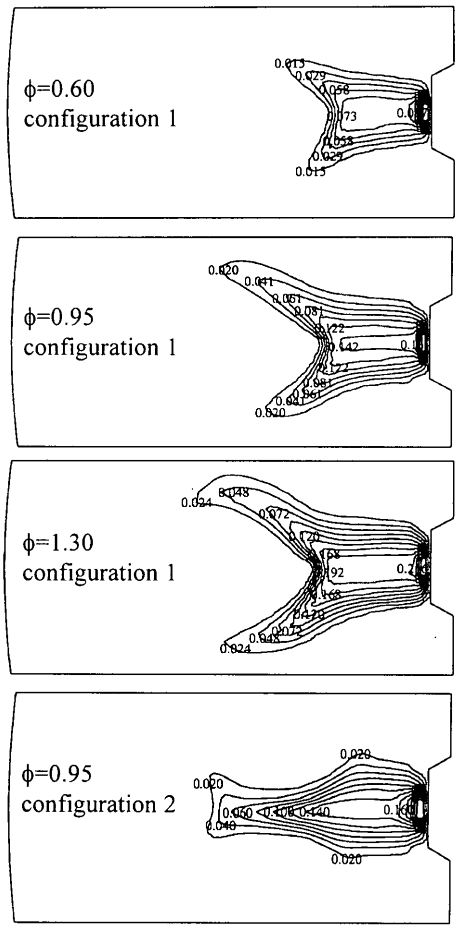

Fig. 5 Fuel mass fractions for various equivalence ratios on top-view midplane

The gas temperature contours on the side and top-view midplanes and exit plane for ϕ=0.95 are shown in Fig.6. The fuel rich mixtures prevailing along the centerline of the primary zone result in relatively low gas temperatures, whereas high temperature regions occur near the edges of the spray. In the case of configuration 2, vaporized fuel can travel far downstream of the air jets from the primary hole because the air jets are not in line with the fuel injector. Therefore, high temperature regions are still found in the intermediate zone. Although the temperature contours are similar within the primary zone, very different trends are shown in the intermediate zone for two different configurations. These phenomena are also observed at the top-view midplane. In the exit plane, high temperature regions are found around the side periodic plane in the case of configuration 1. But in the case of configuration 2, high temperature regions are still found around the center, which indicates that the effect of air jets from the primary hole is negligible for the dilution of combustion gas. Therefore, configuration 1 can be recommended for an effective arrangement of primary dilution hole.

Of most interest is the temperature distribution in the exit plane, which is shown in Fig.7. Experimental data [11] were measured at 4.8, 14.5, 29.0, 53.1, 72.5, 87.0, and 96.7 percent of the exit plane height. Corresponding data from numerical calculations for comparision with experiments are mass weighted average values taken along the circumferential direction in the exit plane. In the case of configuration 1, the results show good agreement with the experimental data for both cases. The temperature distribution for the configuration 2 is found to be higher compared with that of configuration 1. This difference is attributed to the poor mixing patterns, as explained previously.

Table 2 shows the maximum and average temperatures and pattern factors in the combustor exit plane. For the configuration 1, the maximum and average temperatures are found to have less than 2% difference compared with the experimental data. But the pattern factors for the cases 1 and 2 obtained from numerical simulations are 20% and 12% higher respectively than the values from experiments due to the under-prediction of mixing phenomena. For the configuration 2, the predicted maximum and average temperatures are 10~33% higher than that of configuration 1 due to the poor jet mixing in the primary zone.

Figure 8(a) shows the mass weighted average temperature distributions in the primary and intermediate zones along the axial direction for various equivalence ratios. It illustrates that the temperature reaches a maximum when the equivalence ratio in primary zone is near the stoichiometric value. In the fuel rich or lean mixtures, relatively lower temperature is observed in the primary zone due to incomplete combustion. The variations of average exit temperature with respect to the equivalence ratio are also shown in the Fig.8 (b). The exit temperature increases linearly proportional to the equivalence ratio. This is due to the existence of unburned fuel in the primary and intermediate zones which leads to an increase of temperature far downstream.

5. CONCLUSIONS

A three dimensional, curvilinear, multi-domain CFD analysis has been performed on the reverse flow annular gas turbine combustor. Two configurations of primary holes were examined. Configuration 1 in which the primary jets are located in the midplane is recommended for the good jet mixing. Simulations were also performed at two operating conditions for various fuel mass flowrates. It is found that as the mass flowrate of fuel increases, the average exit temperature increases. In addition, the primary zone temperature reaches a maximum value when the equivalence ratio is near stoichiometric value. For the configuration 1, the maximum and average temperatures in the combustor exit have less than 2% difference compared with experimental data, but pattern factors for the cases 1 and 2 are over-predicted by 20% and 12%, respectively.

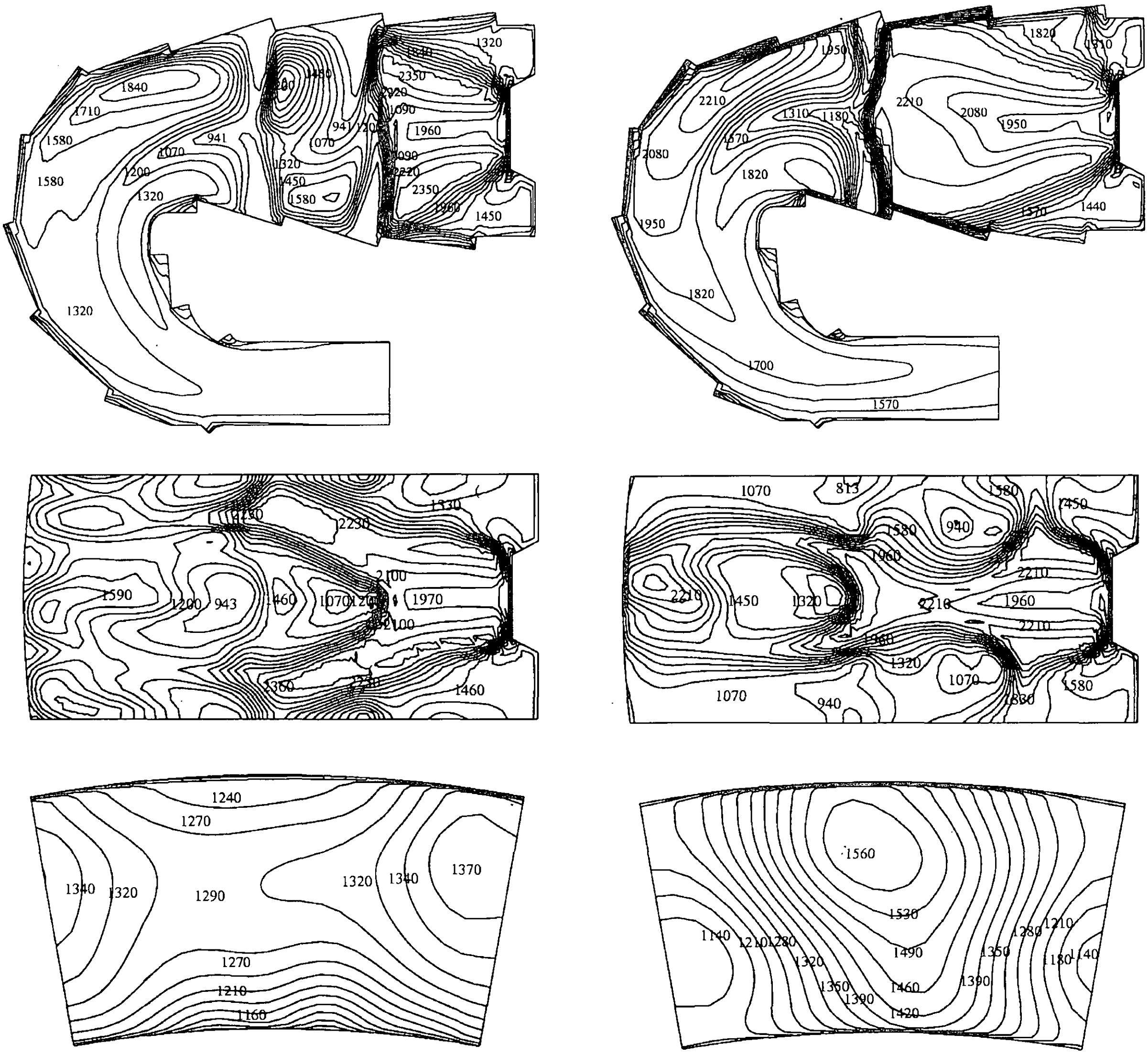

(a) Configuration 1

(b) Configuration 2

temperature units (K)

Fig. 6 Temperature contours for ϕ=0.95 on side and top-view midplanes and exit plane

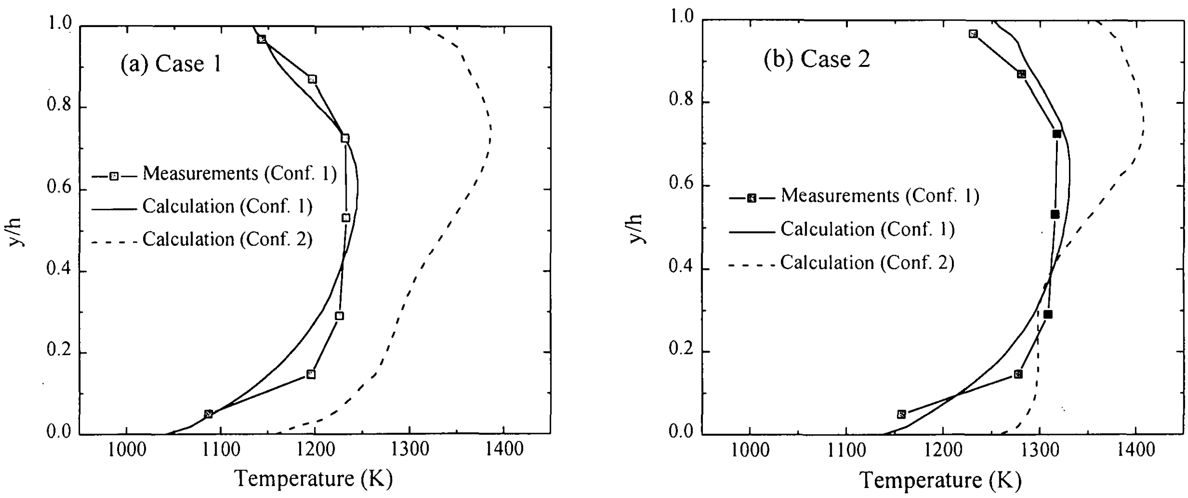

Fig. 7 Radial temperature profiles in exit plane for ϕ=0.95

Table 2. Maximum and average temperatures and pattern factors

		Meas. Conf.1	Calc. Conf. 1	Calc. Conf. 2
Case 1	Max. Temp. (K)	1301	1312	1583
	Avg. Temp. (K)	1201	1193	1321
	Pattern factor	0.162	0.195	0.355
Case 2	Max. Temp. (K)	1387	1405	1603
	Avg. Temp. (K)	1284	1289	1344
	Pattern factor	0.173	0.193	0.394

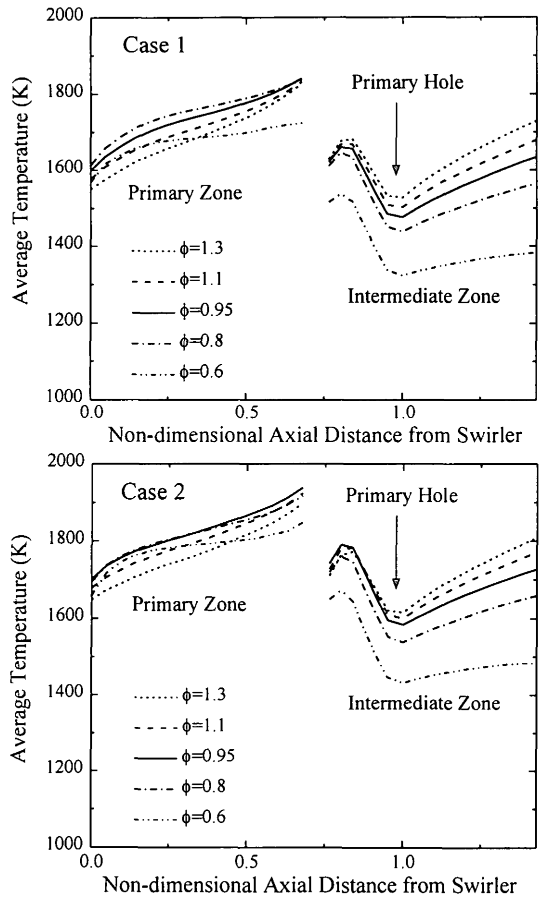

(a) average temperature along the combustor

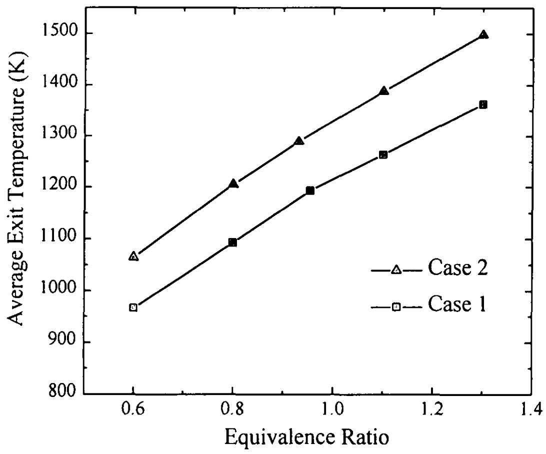

(b) Average exit temperature

Fig. 8 Variations of average temperature with respect to equivalence ratio

6. NOMENCLATURE

$C_{p\ell}$	specific heat of the droplet (J/kg-K)
h	heat transfer coefficient (W/m^2-K)
h_{fg}	latent heat (J/kg)
T_ℓ	temperature of droplet (K)
T_{max}	maximum combustor exit temperature (K)
T_{ex}	average combustor exit temperature (K)
T_{in}	average combustor inlet temperature (K)
θ_R	radiative temperature ($\theta_R^4 = I/4\sigma$) (K)
I	radiation intensity (W/m^2)
σ	Stefan-Boltzmann constant (5.67× 10^{-8}W/m^2-K^4)

7. REFERENCES

1. Fuller E.J. and Smith C.E., Integrated CFD Modeling of Gas Turbine Combustors, AIAA-93-2196.
2. Tolpadi A.K., Calculation of Two-Phase Flow in Gas Turbine Combustors, Journal of Engineering for Gas Turbines and Power, Vol.117 (1995), pp.695-703.
3. Tolpadi A.K., Hu I.Z., Correa S.M. and Burrus D.L., Coupled Lagrangian Monte Carlo PDF-CFD Computation of Gas Turbine Combustor Flowfields With Finite-Rate Chemistry, Journal of Engineering for Gas Turbines and Power, Vol.119 (1997), pp.519-526.
4. Crocker D.S., Nicholaus D. and Smith C.E., CFD Modeling of a Gas Turbine Combustor From Compressor Exit to Turbine Inlet, Journal of Engineering for Gas Turbines and Power, Vol.121 (1999), pp.89-95.
5. Fuller E.J. and Smith C.E., CFD Analysis of a Research Gas Turbine Combustor Primary Zone, AIAA-94-2768.
6. Tolpadi A.K., Burrus D.L. and Lawson R.J., Numerical Computation and Validation of Two-Phase Flow Downstream of a Gas Turbine Combustor Dome Swirl Cup, Journal of Engineering for Gas Turbines and Power, Vol.117 (1995), pp.704-712.
7. Rizk N.K., Chin J.S. and Razdan M.K., Modeling of Gas Turbine Fuel Nozzle, Journal of Engineering for Gas Turbines and Power, Vol.119 (1997), pp.34-44.
8. Datta, A. and Som, S.K., Effects of Spray Characteristics on Combustion Performance of a Liquid Spray in a Gas Turbine Combustor, Int. J. Energy Res., Vol.23 (1999), pp.217-228.
9. Crocker D.S., Smith C.E. and Myers G.D., Pattern Factor Reduction in a Reverse Flow Gas Turbine Combustor Using Angled Dilution Jets, ASME 94-GT-406.
10. Morsi, S.A. and Alexander, A.J., An Investigation of Particle Trajectories in Two-Phase Flow Systems, J. Fluid Mech., V.55 (1972), pp.193-208.
11. Choi, S.M, Chen, S.B. and Min, S.K., An Experimental Study of the Annular Reverse Combustor I, Proceedings of the KSAS Spring Annual Meeting, (2000), pp.513-517.
12. Choi, S.M, Chen, S.B. and Min, S.K., An Experimental Study of the High Shear Nozzle and Swirler, Journal of the KSAS, Vol.26, No.8 (1998), pp.92-104.